A quasi-dimensional model of heat transfer applied to a diesel engine

A. C. Hansen*

(First received May 1992, Final version October 1992)

Abstract

Heat transfer from the combustion chamber of a diesel engine is due to conduction, convection and radiation, each component making a significant contribution to the total heat loss. The main objective of this reseach was to develop a heat transfer model that included all three modes of heat transfer and that was more physically based than existing zero-dimensional models thereby providing a more accurate foundation for evaluating the combustion and resulting thermal stresses generated in direct injection diesel engines. Results from fired engine tests showed that the model generated combined heat transfer rates that were credible not only on a global basis but also in terms of point predictions in the combustion chamber.

Introduction

The gross heat loss to the coolant during combustion in internal combustion engines normally lies in the range of 10-35% of the fuel energy and depends on engine type, size, efficiency, load and speed [1,2]. Energy is lost from the gases in the combustion chamber thus reducing the amount of piston work and affecting engine performance. Gas temperatures are also affected and through them combustion rate, emissions formation, knock and other related factors. Further areas of importance are the thermal loading of engine structural components and the optimisation of engine cooling systems [3]. The researcher involved in engine design, optimisation of engine performance or investigations of alternative fuels therefore requires a representation of the heat transfer processes that will achieve an acceptable level of accuracy.

Heat losses from the combustion chamber occur as a result of heat transfer from gases to the walls and of heat conduction through the structure and to the coolant. It is generally accepted that, given the correct boundary conditions, the heat conduction portion of the heat losses can be calculated to any desired accuracy using finite element models [3]. Gas-to-wall heat transfer correlations have to rely on models for the processes taking place in the combustion chamber. These correlations in turn are used to establish the boundary conditions for the heat conduction calculations. Hence an accurate description of the heat flux rates and their spatial and temporal variations within the cylinder is very important.

Heat transfer from the gases to the walls is due both to convection and radiation. In the past, greater emphasis was placed on the convection component as radiation was considered by some researchers to contribute a negligible portion of the heat transfer. However, measurements of time-averaged heat transfer indicated that 20-40% of the total cylinder flux was due to radiation [4].

Heat transfer in the combustion chamber of a direct injection diesel engine varies considerably on both a spatial and temporal basis. Heat flux to the surface of the chamber can vary from zero to as high as 10 MW/m^2 and back to zero again in less than 10 ms while portions of a surface only 10 cm apart can receive peak fluxes differing by as much as 5 MW/m^2 [4]. The combination of substantial variations in temperature and pressure of the contents of the combustion chamber and the cyclic movement of the piston leading to varying three-dimensional geometry confronts the researcher with a complex problem.

The evaluation not only of engines but also different fuels in terms of heat transfer effects has received relatively scant attention. Callahan *et al.* [5] selected heat transfer models for ease of programming and adaptability to a wide range of engine-fuel combinations. It could be expected that convective and radiative heat transfer rates with different fuels in the same engine would vary according to fluctuations in gas temperatures. In addition fuel chemical and physical properties would influence the radiative component in terms of soot formation during combustion. For instance an alcohol-based fuel would cause relatively little radiative heat transfer because of a tendency towards clean burning.

The main objective of this research was to develop a heat transfer model that was less empirically based than the existing zero-dimensional models in order to provide a more accurate foundation for evaluating the combustion and resulting thermal stresses generated by alternative fuels in diesel engines. Particular attention was paid to the development of a spatial and temporal model of convective heat transfer that was based on gas flow characteristics. The complete model was formulated in such a way that it could be applied with the aid of a micro-computer. The response of the model to data from a motored engine is described by Hansen [6]. This paper deals with the verification of the model under fired engine conditions.

The advantages of this approach to the modelling were that subsequent heat release computations would be more accurate than achieved with zero-dimensional models and would reflect more closely the influences of combustion chamber geometry with special reference to convective heat transfer. In addition fairly accurate boundary conditions would be generated for structural

* Senior Lecturer (Member), Department of Agricultural Engineering, University of Natal, Pietermaritzburg.

calculations in finite element models, the results of which depend critically on the applied thermal loads. The revised model would still be driven to a large extent by cylinder pressure data and therefore would remain diagnostic in nature.

Formulation of Model

A review of heat transfer and combustion models indicated that single zone models such as those of Eichelberg [7], Annand [8] and Woschni [9], although useful for basic comparisons in diagnostic work, had certain limitations, in particular the lack of spatial resolution, which precluded their successful use in thermal stress analysis, heat transfer and emissions modelling. At the other end of the scale the multi-dimensional models required computing power beyond the micro-computer and were not necessarily more accurate than simpler models [4]. Therefore a model was required which was somewhere between the single zone and multi-dimensional models and which provided some degree of spatial as well as temporal resolution in terms of heat transfer. Zonal models made up of carefully selected and tested submodels should provide a level of accuracy which surpasses that of the global models but which should still generate cost and time effective solutions directly applicable to engineering problems. Models such as those of Morel and Keribar [10] and Szekely and Alkidas [11] were considered to be the closest in meeting these requirements.

Basic Structure

The complete model developed in this study consisted of a number of sub-models representing in-cylinder gas flow processes, heat transfer and combustion. Figure 1 illustrates the structure of the model used to investigate fired engine conditions. Details of the model applied under motored engine conditions were presented by Hansen [6] and therefore only a brief outline of the relevant sub-models discussed by Hansen [6] is provided in this paper. For the modelling of in-cylinder gas flow the combustion chamber volume was divided into an inner cylindrical volume and an outer annular volume shown schematically in Figure 2 [12,13]. Also shown in Figure 2 are the six

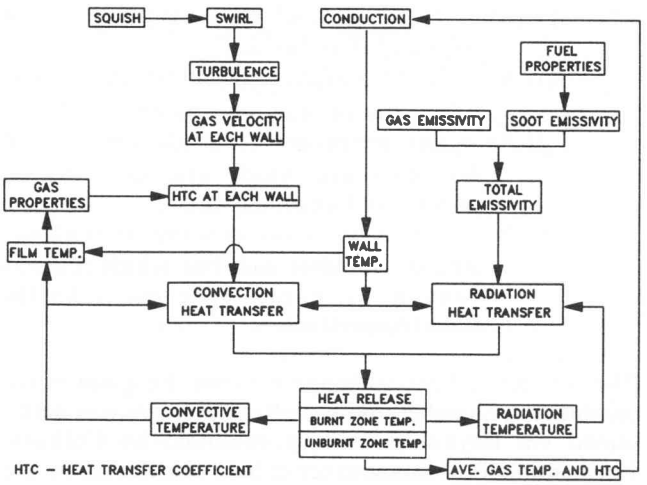

Figure 1 Block diagram showing structure of model.

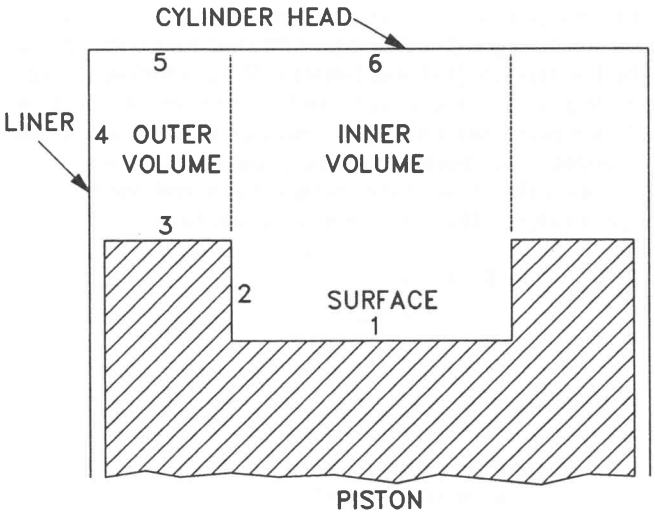

Figure 2 Division of combustion chamber volume into an inner and outer volume and of the chamber surface area into six discrete elements.

discrete surfaces making up the total surface area of the combustion chamber as applied by Morel and Keribar [10].

With reference to the model structure shown in Figure 1 for fired engine conditions, the calculation procedure for the convection heat transfer was the same as for the motored engine case except for the input of a convective temperature based on the combustion process. At each crank angle between inlet valve closing (IVC) and exhaust valve opening (EVO) the in-cylinder gas flow components of squish, swirl and turbulence are employed in the calculation of area-averaged resultant velocities at each of the designated surfaces in the combustion chamber. These velocities in conjunction with the gas properties of the boundary layer determine the convective heat transfer coefficients.

A sub-model of radiation heat transfer is included which in turn requires the input of total emissivity, wall temperature and a radiation temperature which is also based on the combustion process. The total emissivity is made up of two components resulting from gas radiation and soot radiation respectively. The calculation of soot emissivity requires the input of fuel properties. The computation of wall temperature is performed with the aid of a conduction model and an iterative procedure as for the motored engine case.

The heat release model into which the convection and radiation heat transfers were fed was adapted from an existing heat release model so that a burnt products zone and an unburnt zone were generated during the course of combustion. The temperatures of each zone were then used in the calculation of the convective and radiation temperatures. The measured pressure was required in the calculation of the bulk gas temperature and of the rate of heat release.

Two-Zone Combustion Model

A quasi-dimensional burnt zone model based on the model formulated by Morel and Keribar [10] was developed

for this analysis. An existing single zone model founded on the Krieger-Borman equation that had been applied by Faletti *et al.* [14] and Taylor [15] was modified to generate a burnt zone volume and to take into account the flow-based convective heat transfer and radiation heat transfer. The thermodynamic cycle code in this model supplied the mass of the burned gases and the bulk gas temperature. Then from the ideal gas law:

$$P_b.V_b = m_b.R_b.T_b \quad \text{..... (1)}$$

$$P_u.V_u = m_u.R_u.T_u \quad \text{..... (2)}$$

$$P_t.V_t = m_t.R_t.T_t \quad \text{..... (3)}$$

where P = pressure, kPa
V = volume, m^3
m = mass, kg
R = gas constant, kJ/kg.K
T = temperature, K
subscript b = burnt zone
u = unburnt zone
t = total cylinder contents

Pressure and the gas constant were assumed to be the same throughout the cylinder.

$$\text{Hence } R_b = R_u = R_t \quad \text{..... (4)}$$

$$\text{and } P_b = P_u = P_t \quad \text{..... (5)}$$

$$\text{And also } m_b + m_u = m_t$$

$$\text{and } V_b + V_u = v_t$$

From equations (1), (2) and (3) it can be shown that:

$$T_t = \frac{P_t.V_t}{m_t.R_t} = P_t.\left(\frac{V_u + V_b}{m_t.R_t}\right)$$

$$= P_t.\left(\frac{m_u.R_u.T_u/P_u + m_b.R_b.T_b/P_b}{m_t.R_t}\right)$$

Simplifying with equations (4) and (5):

$$T_t = (m_u.T_u + m_b.T_b)/m_t$$

$$\text{Hence } T_b = (m_t.T_t - m_u.T_u/m_b$$

Substituting for m_u and re-arranging:

$$T_b = T_u + (T_t - T_u)/(m_b/m_t) \quad \text{..... (6)}$$

The bulk gas temperature T_t in equation (6) was obtained from the thermodynamic cycle code. The temperature of the unburnt zone T_u was generated from a sub-model relying on the First Law of Thermodynamics and taking into account heat transfer from the burnt zone to the unburnt zone. The ratio of the instantaneous burnt mass of gas to the total mass of gas in the cylinder, m_b/m_t was determined by tracking the production of CO_2 specified as one of the species in the gas mixture and comparing it to the total mass of CO_2 that would have been generated under stoichiometric conditions. The burnt volume V_b could then be determined from equation (1).

The fixed geometry of the burnt volume permitted the calculation of the surface area at the interface between the burnt and unburnt zones. This surface area, the temperature difference between the two zones and an adjustable constant representing a gas-to-gas heat transfer coefficient were used in the calculation of heat transfer from the burnt to the unburnt zone. The constant was adjusted so that the peak temperature of the burnt zone did not exceed the adiabatic flame temperature.

The temperatures and masses of the burnt and unburnt zones as well as the geometry of the burnt zone were used in the calculation of the convective and radiation heat transfer components. Following a similar procedure to that of Morel and Keribar [10] a convective temperature, T_{cg} was calculated for each of the regions shown in Figure 2.

In-Cylinder Gas Flow

The gas flow characteristics in the combustion chamber of a direct injection (DI) diesel engine during the compression and expansion strokes is governed primarily by piston velocity, squish, swirl and turbulence intensity. The variation of squish and swirl during the cycle is determined by the conservation of mass and angular momentum. Turbulence intensity, which is more difficult to model accurately than squish or swirl, was computed from a model of turbulence with its roots in the Navier-Stokes equations. The area-averaged velocities were based on contributions from piston motion, squish, swirl and turbulence. The formulation and verification of these gas flow models have been discussed in detail by Hansen [16,17] and therefore are not covered any further.

Convective Heat transfer

The procedure used for determining the convective heat transfer was similar to that of Morel and Keribar [10] based on a model representing the effects of gas flow. The starting point for this model was the instantaneous heat flux equation:

$$q_c(t,A) = h_c(t,A).[T_{cg}(t,A) - T_w(A)] \quad \text{..... (7)}$$

where $q_c(t,A)$ = heat flux which varies as a function of time and chamber wall
$h_c(t,A)$ = heat transfer coefficient which varies as a function of time and chamber wall
$T_{cg}(t,A)$ = gas temperature outside the thermal boundary layer which varies as a function of time and chamber wall
$T_w(A)$ = wall temperature which varies as a function of chamber wall but which remains constant within each cycle, except for the liner temperature.

The convective heat exchange between the gases in the combustion chamber and the chamber walls was determined via Reynolds' analogy modified by Colburn. Further details of this convective heat transfer model are given by Hansen [6].

Conductive Heat Transfer

The objective in formulating a conduction model was to provide temperatures at each of the six designated surfaces in the combustion chamber that were of the right order of magnitude and that were linked to the operating conditions. The latter conditions included engine speed, load, coolant and oil temperatures. However, it was also important to provide a relatively simple model generating an output with acceptable accuracy.

After studying published results of temperature distributions in the combustion chamber components certain guidelines were established for preparing a conduction model. First of all the combustion chamber was divided into the three main components of piston, liner and cylinder head. The inlet and exhaust valves were treated as being part of the head and the conditions in the head were adjusted to account for temperature differences that would have been caused by the valves and ports, particularly the exhaust valves which is generally at a somewhat higher temperature than the cylinder head. The heat transfer through each of the three components was assumed to be one-dimensional and steady state and was represented by resistance networks. The resistance network at each one of the six surfaces consisted of two thermal resistances representing the gas-to-wall convection resistance in the combustion chamber and the combined conduction and convection resistance from the wall through to either the coolant in the case of the liner and head or the oil in the case of the piston. Further information on this conductive heat transfer model was presented by Hansen [6].

Radiation Heat Transfer

The model for radiation was selected so that it would be sufficiently complex so as to take into account fuel properties and equivalence ratio but not so sophisticated as to require substantial computations. A similar model as applied by Callahan *et al.* [5] was used. This model was based on work by Kunitomo *et al.* [18] subsequently modified by Kamel and Watson [19]. The radiant heat flux was calculated from the well established equation:

$$q_r(t,A) = \varepsilon_f(t).\sigma.\{[T_{rg}(t,A)]^4 - [T_w(a)]^4\} \quad \ldots (8)$$

where $q_r(t,A)$ = radiation heat flux which varies as a function of crank angle and chamber wall
$\varepsilon_f(t)$ = flame emissivity which varies as a function of crank angle
σ = Stefan-Boltzmann constant
$T_{rg}(t,A)$ = radiation temperature which varies as a function of crank angle and chamber wall
$T_w(A)$ = wall temperature as previously defined.

There are two main sources of radiation in the combustion chamber of a diesel engine, soot and certain gases. The flame emissivity represents a combination of these two components. By assuming that the total absorption coefficient was the sum of the absorption coefficients of the gas and soot, Chang and Rhee [20] derived the equation:

$$\varepsilon_f = 1 - (1 - \varepsilon_s).(1 - \varepsilon_g) \quad \ldots (9)$$

Non-luminous radiation from the combustion gases is mainly due to emission contributions from the triatomic molecules of carbon dioxide and water vapour. The total gas emissivity can be calculated from the following approximation:

$$\varepsilon_g = 1 - (1 - \varepsilon_{CO_2}).(1 - \varepsilon_{H_2O}) \quad \ldots (10)$$

Callahan *et al.* [5] applied the equations put forward by Kamel and Watson [19] for evaluating the gas emissivities. For a particular gas i:

$$\varepsilon_i = 1 - \exp(-K_i.p_i.L) \quad \ldots (11)$$

where ε_i = emissivity of gas i
K_i = mean absorption coefficient of gas i
P_i = partial pressure of gas i
L = mean radiation length.

The mean absorption coefficients for CO_2 and H_2O were calculated using equations from Kamel and Watson [19] which represented curve fits to graphs presented by Abu-Romia and Tien [21]. Callahan *et al.* [5] stated that these equations were only valid for gas temperatures between 800 K and 1950 K:

$$K_{CO_2} = 1{,}02 - 1{,}11\left[\frac{T_g}{1\,000}\right] + 0{,}422\left[\frac{T_g}{1\,000}\right]^2 - 0{,}05368\left[\frac{T_g}{1\,000}\right]^3$$

$$K_{H_2O} = 0{,}52 - 0{,}888\left[\frac{T_g}{1\,000}\right] + 0{,}5266\left[\frac{T_g}{1\,000}\right]^3 - 0{,}1043\left[\frac{T_g}{1\,000}\right]^3$$

The partial pressures of the gases at each crank angle increment, $P_i(\theta)$ were computed from the mass fraction of fuel burned, $X(\theta)$, the molar fraction of the respective gas, $y_i(\theta)$ and the total gas pressure $P(\theta)$:

$$p_i(\theta) = X(\theta).y_i(\theta).P(\theta)$$

Callahan *et al.* [5] approximated the mean radiation length using the definition proposed by Kunitomo *et al.* [18]:

$$L = 3{,}5\frac{V(\theta)}{A(\theta)}$$

where $V(\theta)$ = instantaneous volume
$A(\theta)$ = instantaneous surface area of combustion chamber

The procedure used to calculate soot emissivity was the same as developed by Kunitomo *et al.* [18] and applied by Callahan *et al.* [5]. Soot emissivity at atmospheric pressure was related to gas emissivity at atmospheric pressure which was obtained from the following equations of Kamel and Watson [19]:

$$\varepsilon_{CO_2} = 0{,}711(p_{CO_2}.L/100)^{0.333}/(T_g/100)^{0,5} \quad \text{..... (12)}$$

$$\varepsilon_{H_2O} = 0{,}707(p_{H_2O}.L/100)^{0,6}.(p_{H_2O}/100)^{0,2}/(T_g/100) \quad \text{... (13)}$$

where p_{CO_2} and p_{H_2O} = partial pressures, kPa
L = mean radiation length, m
T_g = bulk gas temperature, K.

The total gas emissivity at atmospheric pressure ε_{ga} was calculated from equation (10). The soot emissivity at room temperature was obtained from an empirical equation developed by Kunitomo *et al.* [18]:

$$\varepsilon_{sa} = \varepsilon_{ga}.\left(\frac{0{,}09}{\phi_o^2 - \tau^2 + 0{,}35\tau - 0{,}38 + 6{,}8\tau - 5{,}95}\right) \quad \text{..... (14)}$$

where τ = specific gravity of the fuel
ϕ_o = effective excess air ratio.

Callahan *et al.* [5] provided a graph of the effective excess air ratio versus specific gravity. They indicated that a significant amount of data showed that the effective excess air ratio was fairly insensitive to specific gravity and that more data were required to verify the relationship at higher specific gravities.

The soot emissivity at room temperature in equation (14) was used to calculate a mean absorption coefficient:

$$K_{sa} = \frac{-1}{L}.\log(1 - \varepsilon_{sa})$$

Kunitomo *et al.* [18] provided an empirical equation for determining the mean absorption coefficient at a given pressure:

$$K_s = K_{sa}.\left(\frac{P}{100}\right)^m$$

where P = total cylinder pressure, kPa
$m = 4{,}95/(\phi_o + 1{,}5) - 0{,}25.$

The soot emissivity at the given pressure was finally determined from the equation:

$$\varepsilon_s = 1 - \exp(-K_sL)$$

The flame emissivity in equation (9) could therefore be calculated from the gas and soot emissivities and substituted into equation (8) for computing the heat flux.

The radiation temperature in equation (8) has been represented by researchers with values varying from the adiabatic flame temperature to the bulk gas temperature. The procedure used for this work was based on the model applied by Morel and Keribar [22] in which the radiation temperature T_{rg} was linked to the average temperature of the burned zone T_b. After the start of combustion up to the point of maximum temperature in the burned zone, $T_{rg} = 0{,}9T_b$. This was done by Morel and Keribar [22] to account for the preferential radiant heat transfer from the soot particles which were thus cooler than the surrounding burned gases. After the point of maximum temperature the radiation temperature was determined from an equation similar to that used by Morel and Keribar [22]:

$$T_{rg} = 0{,}9[T_{b,max} + (T_b - T_{b,max})(\theta - \theta_{max})/(\theta_{EVO} - \theta_{max})] \quad \text{(15)}$$

where $T_{b,max}$ = maximum burnt temperature
θ = instantaneous crank angle
θ_{max} = crank angle at $T_{b,max}$
θ_{EVO} = crank angle at EVO

This form of equation was adopted by Morel and Keribar [22] to account for the fact that due to the fourth power temperature dependence of radiation the effective soot radiating temperature was dominated by the actively burning flame front, the temperature of which was higher than the average of the burned zone. Temperature of the burned zone was affected by the presence of burned-out products and by air entrainment.

Equation (15) causes the radiation temperature to decrease almost linearly from the maximum value to a value close to the bulk gas temperature in accordance with the variations in temperature predicted by Borman and Nishiwaki [4]. This variation is illustrated in Figure 3 for a load of 200 Nm at rated speed on an ADE 236 engine. This relationship was chosen over that of Morel and Keribar [22] as the latter relied on a factor which was proportional to the square of the ratio of burnt mass to total mass. In the present model the ratio of burnt mass to total mass does not reach a value of one thus causing the radiation temperature at the tail end of combustion to be higher than the bulk gas temperature. Nevertheless the calculation of T_{rg} in equation (15) is still linked to the variation of T_b.

The same wall temperature values as for the convective heat transfer calculation were applied in equation (8). Hence the radiative heat transfer combined with the convective heat transfer provided the total heat transfer to be used in the calculation of fuel energy release rates.

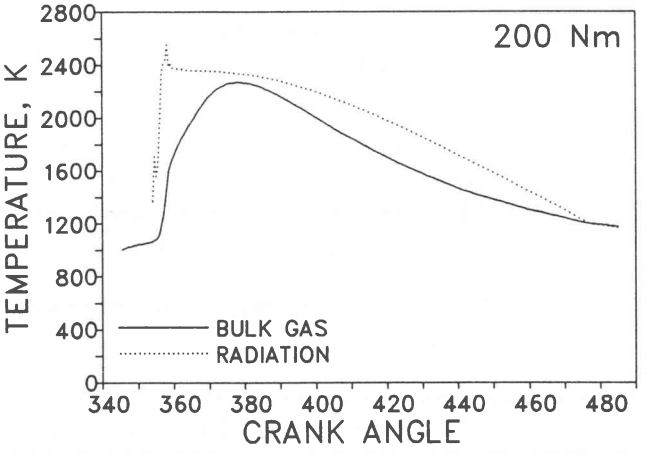

Figure 3 Variation of radiation temperature with crank angle at an engine load setting of 200Nm at 2200 r/min.

Equipment and Test Procedure

As the model was diagnostic in nature it was difficult to rely on published data to verify the heat transfer predictions without being able to generate the actual combustion pressure conditions in the cylinder. Apart from measurements of cylinder pressure, a heat flux probe was used to monitor variations in surface temperature which were then converted into heat flux. The probe and the data processing techniques were developed by Taylor *et al.* [23] and for this work remained the same except where indicated.

The data were obtained from a four-cylinder naturally aspirated ADE 236 engine. All the dimensions including the piston crown-to-head clearance at TDC and the compression ratio were based on actual measurements in the engine. The engine was mounted on a test bed with a conventional cooling system. Air flow rate into the engine was measured accurately with the aid of a parabolic orifice at the air inlet in conjunction with a surge chamber to eliminate pulsations. Steady state temperatures that were measured on the engine included oil temperature, coolant temperature, exhaust temperature and inlet air temperature, which was monitored close to the inlet valve.

The cylinder at the front of the engine opposite to the flywheel was instrumented with a Kistler 6121 pressure transducer mounted flush with the cylinder head and situated just inside the piston bowl area as shown in Figure 4. The heat flux probe was designed and developed by Taylor *et al.* [23] in such a way that it could be installed in the engine in place of the pressure transducer.

Injection timing was determined from the signal of a needle lift transducer of the inductive type and crank rotation was monitored with an optical shaft encoder attached to the front of the engine and providing a TDC reference and pulses at each half degree crank angle increment. These pulses were used to trigger the data acquisition system. Engine speed was determined from the frequency of the TDC pulses.

A multi-channel data acquisition system described by Hansen *et al* [24] was used to monitor and record the signals emanating from the range of transducers. The system provided a means of recording both high speed and steady state variables as well as displaying, processing and storing data.

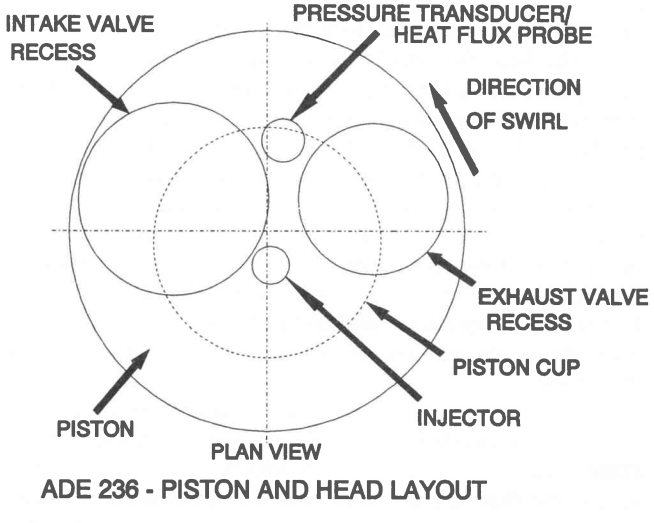

Figure 4 A plan view of the position of the pressure transducer in relation to the cylinder head, valves and piston bowl.

A rigorous calibration procedure was performed before the test to ensure that the measurements were accurate. Calibration checks were also carried out after the test to isolate any change in the response of the instrumentation. The engine was warmed up until the thermostat for regulating the flow of the coolant had opened.

After noting ambient pressure and temperature, steady state and high speed data were recorded systematically at a number of points within the torque-speed range of the engine. Data were collected initially at the rate speed of 2200 r/min with the torque varying from zero to 200 Nm in steps of 50 Nm. The load was then maintained at 200 Nm and the speed was reduced from 2200 r/min to 1400 r/min in steps of 200 r/min. By using this test pattern the model could be checked for conditions of both varying load and constant speed, and varying speed and constant load. At each one of these test points a total of 90 consecutive cycles of high speed data were captured and averaged in addition to the steady state data. Using the window facility of the data acquisition system, the high speed data were captured only during the compression and expansion strokes.

The same test procedure was then repeated with the heat flux probe installed. However, a total of 90 full cycles, each consisting of two engine revolutions, were captured and avaraged at each engine setting along with the steady state data.

Results and Discussion

In the final phase of model verification the combination of the heat transfer models was examined under fired engine conditions. The verification was approached via two routes. The first route involved an analysis of the energy balance taking into account the energy release from the fuel and the heat transfer as compared to the energy input from the fuel. This analysis therefore provided a means of verifying the overall heat transfer from the combustion chamber linked to the combustion of the fuel. The second route was a comparison of the predicted and measured heat transfer at the heat flux probe.

Before proceeding with the details of the energy balance it is pertinent to illustrate the relative contributions of the convective and radiative heat transfers. Figure 5 shows the radiation, convection and total heat transfer rates at rated speed and 200 Nm. The radiation heat transfer forms close to 30% of the total heat transfer between IVC and EVO. This figure is in line with the predictions of a number of researchers. In addition the relative shapes of the curves in Figure 5 are in agreement with published results. Hence it was concluded that the convection and radiation heat transfer models were generating values that were of the right proportion and distribution relative to crank angle.

The variable of particular relevance to the energy balance determined at each engine load and speed was the percentage of fuel mass burnt. This percentage represented the ratio of calculated fuel mass accounted for by the combustion model to the measured fuel mass injected into the cylinder.

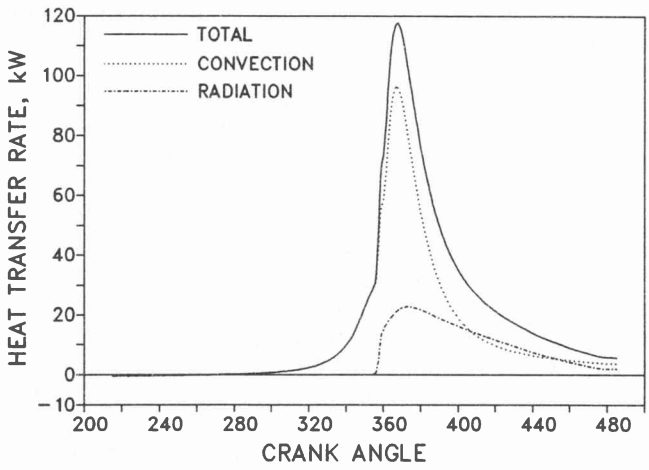

Figure 5 The variation of the radiation, convection and total heat transfer rates with crank angle at rated speed and 200 Nm.

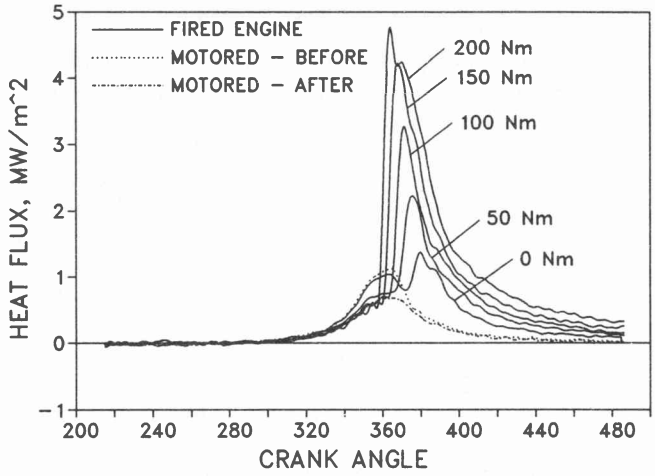

Figure 6 Variation of measured heat flux with crank angle for different loads and for a motored engine at 2200 r/min.

At the constant load of 200 Nm and with varying speed the percentage was between 98 and 99% for the speed range of 1400 to 1800 r/min. This consistency close to 100% also indicated consistency in the prediction of heat transfer with varying speed. It also indicated that practically all the heat transfer was represented by the models. From 1800 to 2200 r/min the percentage decreased to 93,6 which, although relatively low, was still regarded as being acceptable.

The variation of the percentage of fuel mass burnt with load at constant speed was consistent for the torque range of 150-200 Nm at approximately 94%. There was a slight increase at 100 Nm to 95.4% and then a significant decrease to 91% at 50 Nm. This latter decrease was attributed mainly to inconsistent combustion and irregular injection at the low load setting.

While the energy balance was selected as the most suitable method of evaluating the overall prediction of heat transfer in this project, it was recognised that the tests had been carried out in a four cylinder engine with combustion being monitored in only one cylinder at the front of the engine. Hence it was assumed that the fuel was equally distributed among all four cylinders and that the indicated mean effective pressure generated in each cylinder was equal. Differences in these variables between cylinders could account for the variations in percentage of fuel mass burnt at the different loads and speeds. However, the energy balance still provided a useful verification of the overall heat transfer. The objective of the project was to provide a diagnostic model and therefore it should be applicable to production engines such as the ADE 236 engine used in this project.

Verification of the predicted heat transfer with the heat flux probe measurements was carried out with the resultant gas velocities at the probe site being specified as for the motored engine heat transfer predictions. The soot deposits caused by combustion had a significant influence on the heat flux measured at the probe. Therefore it was necessary to take into account the attenuation of the heat flux caused by the deposits. By comparing the heat flux before the start of combustion with the motored engine heat flux before and after the fire engine tests it was possible to establish the history of the soot deposition during the fired engine tests.

The effect of the soot deposition is best illustrated by examining the heat fluxes at 2200 r/min which are presented in Figure 6. Included in Figure 6 are the motored engine heat fluxes before and after the fired engine tests. It can be seen that the motored engine heat flux measured before correlates well with the heat flux measured with the engine idling at 2200 r/min. However, thereafter there is a distinct attenuation of all the curves before the start of combustion for the higher loads and in these cases the motored engine heat flux measured after the fired engine tests correlates well. This result implied that the initial deposits of soot had a significant effect on the heat flux but thereafter, assuming that further deposition did take place, no further attenuation of the heat flux occurred. The close correlation between the motored engine heat flux after the fired engine tests and the portion of the heat flux measured before the start of combustion at constant load with varying speed also supported this observation. The attenuation of the heat flux by the soot deposits was counteracted by amplifying the heat flux measurements so that acceptable agreement with the predicted heat flux was achieved during the compression stroke. The predicted heat flux was determined using the same resultant velocity as computed for the motored engine tests. The latter predictions had been shown to correlate very closely with the measured heat flux from the clean probe [6].

As the heat flux probe was positioned just inside the bowl perimeter and therefore was exposed to the combustion events in the piston bowl and to radiation from the products of combustion it was necessary to incorporate radiation heat transfer into the total heat flux predicted at the probe site. In this case the area-averaged radiation heat transfer was used. In addition the convective temperature computed for the inner volume was applied in the calculation of convective heat transfer at the probe. The wall temperature specified in these calculations was the same as the average surface temperature measured at the probe.

A comparison of the predicted and measured heat fluxes can be made by examining Figure 7. In each of the graphs three curves are shown which represent the measured heat flux, the predited heat flux computed with the convective temperature for the inner volume and the predicted heat flux computed with the burnt zone tempera-

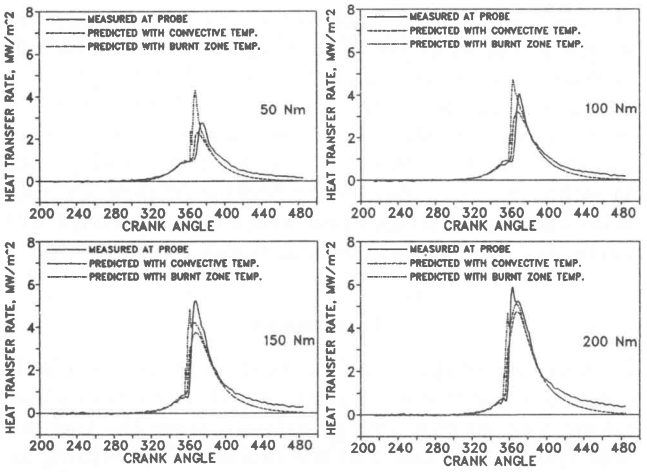

Figure 7 The predicted and measured heat fluxes varying with crank angle for four different loads at rated speed.

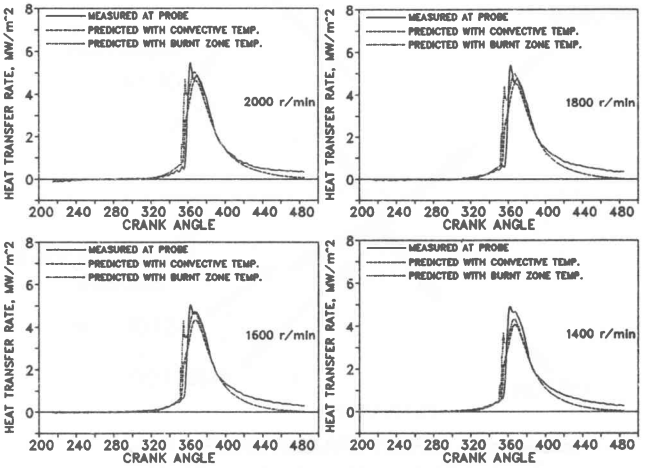

Figure 8 The predicted and measured heat fluxes varying with crank angle at 200 Nm for four engine speeds.

ture. The graphs in Figure 7 which are for constant speed and varying loads show some significant points of deviation of the predicted values from the measured values. The first point of deviation was the crank angle at which the heat flux increased sharply as a result of the start of combustion. At all test points the rise in the measured heat flux was retarded compared to the predicted heat flux. However, the initial rates of increase of flux for the predicted and measured values were almost identical.

The second significant difference was the peak heat flux reached. Again in all cases the model predicted a lower peak than the measured flux based on the convective temperature. In addition the heat flux measured at 2200 r/min and 200 Nm exhibited a prominent narrow peak followed by a second much smaller peak. Double peaks were also exhibited in the fluxes measured at 200 Nm with varying speed as shown in Figure 8. Annand and Ma [25] reported double peaks in their measurements of heat flux and associated them with the premixed and diffusion phases of combustion. Dent and Sulaiman [26] observed the influences of the two stages of combustion in their heat flux data as well.

An initial study of the present set of data suggested that the two stages of combustion were responsible for both peaks. However, a closer examination of the heat fluxes measured at constant load and varying speed showed that the first peaks were all occurring within the narrow range of 362,5° to 365°CA. The positions of the peak rates of heat release at the same speed for the same load varied between 355°CA and 358°CA. The initial sharp rise in measured heat flux at 1400 r/min and 200 Nm was retarded relative to the predicted rise in heat flux by less than 2,5°CA. At 2200 r/min and 200 Nm this retardation was approximtely the same. Hence in these measurements it was concluded that the first peak in the heat flux was not directly linked to the premixed phase of combustion.

An investigation of the peak heat fluxes for the motored engine tests at the same speeds for the clean probe indicated that these peaks also fell within a narrow band of 363° and 365°CA which corresponded very closely to the range observed for the first peak heat fluxes in the fired engine tests. The following explanation is put forward for the trends observed in the measured heat fluxes.

Starting off with the load setting of 50 Nm at 2200 r/min, injection timing was retarded and therefore start of combustion was somewhat retarded. A single peak of heat flux occurred which, taking into account the further retardation of the rise in measured heat flux, coincided with the end of the premixed phase and therefore with what could be regarded as the maximum rate of diffusion combustion. Increasing the load to 100 and 150 Nm resulted in the same single peak in each case but with corresponding increases in peak values. The peak heat flux at 150 Nm took place just before 370°CA. Again these peaks corresponded to the peaks in diffusion combustion rates.

At 2200 r/min and 200 Nm the start of combustion had advanced sufficiently so that the heat flux started to rise sharply after combustion just before TDC. This rise also signified a substantial rise in cylinder pressure. The result was that as the piston started its descent from TDC the reverse squish that was generated was boosted further by the hot, high pressure combustion gases flowing into the cooler, low pressure zone sandwiched between the piston crown and head. The boosted reverse squish then caused an increase in the heat flux particularly in the case of the measurements at the probe, which was situated at a point in the head where the hot gases were likely to impinge as they found their way from the piston bowl into the clearance volume. The same reasoning could be applied to the measured heat fluxes shown in Figure 8.

The differences in the crank angles at which the heat fluxes began to rise after the start of combustion as well as the differences in the predicted and measured peak heat fluxes could be attributed partly to the location of the fuel spray plumes. Annand and Ma [25] and Van Gerpen *et al.* [27] stated that the position of the fuel spray plume relative to the surface thermocouple could have a significant effect on the measured heat flux.

An examination of the trajectories of the spray plumes for the ADE 236 engine indicated that there was one plume upstream of the probe relative to the direction of swirl. Figure 9 illustrates the approximate positions of the plumes compared to the head. The injection of fuel upstream of the probe would have meant that there would have been a time delay before the fuel reached the vicinity of the probe and also started burning. This factor was

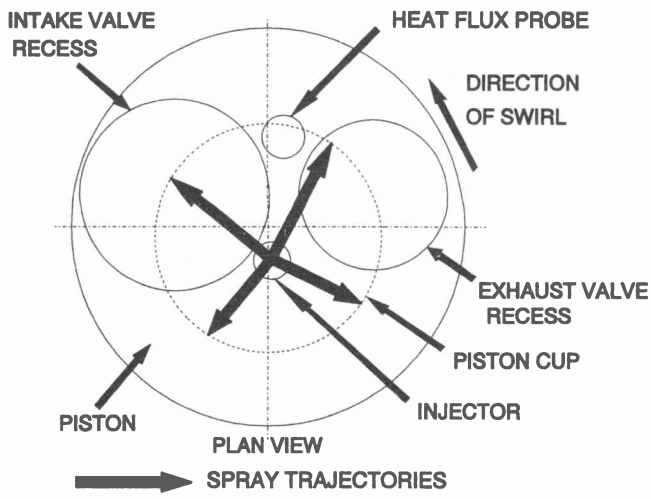

Figure 9 The plan view of the cylinder head and piston showing the approximate trajectories of the spray plumes.

regarded as the main cause of the delayed response of the probe.

The effect of the position of the spray plumes highlighted the heterogeneous form of the combustion and therefore the localised differences in conditions in the combustion chamber. These differences were also likely to apply to the gas temperatures. It could be said that the temperatures at the probe could vary from the unburnt zone temperature to the burnt zone temperature as combustion took place. Therefore, for comparative purposes, the predicted heat flux based on the burnt zone temperature was included in Figure 7. At the lower loads of 50 and 100 Nm and the rated speed it was possible that an intermediate temperature between the convective temperature and the burnt zone temperature would be applicable. At 150 Nm even the predicted peak heat flux using the burnt zone temperature fell slightly short of the measured peak heat flux. Nevertheless there was better correspondence when the burnt zone temperature was used.

The peak heat flux predicted by the burnt zone temperature in Figure 7 remains approximately the same in all four graphs in spite of the change in load. This results is attributed to the temperature of the burnt zone increasing rapidly after the start of combustion to a maximum which is approximately the same as the adiabatic flame temperature under stoichiometric conditions. The maximum temperature of the burnt zone in the premixed phase and therefore the heat flux remain approximately the same for the load range illustrated in Figure 7.

At 200 Nm and 2200 r/min as well as at the lower speeds there was much closer agreement in the peak heat fluxes taking into account the temperature range being considered for the calculation of the predicted heat flux. It was therefore concluded that, apart from the selection of the appropriate gas temperature, the model was providing acceptable predictions of heat flux that were linked to the gas flow characteristics.

The results show that, using fired engine data, the model generates heat transfer rates which can be defended not only on a global basis where the heat transfer rates through designated surfaces are averaged, but also in terms of point predictions in the combustion chamber. The results also highlight the considerable variation in heat transfer that can occur from one point in the chamber to another. Such variations add considerable weight to the objective of moving away from a zero-dimensional model to a quasi-dimensional type where some predictions can be made on a more localised rather than global basis. For this type of prediction the well established global heat transfer models of Annand [8] and Woschni [9] are inappropriate because of their formulations and the variables upon which they are based with particular reference to the heat transfer coefficients.

Conclusions

In this phase of the model verification process where the combined heat transfer was examined, an energy balance taking into account energy released from the fuel and heat transfer showed that the model was providing acceptable predictions of the total heat transfer from the combustion chamber.

Predictions of heat flux at the probe did not approach the same level of agreement with measured heat flux as achieved under motored engine conditions. Nevertheless when compared to the correspondence of measured and calculated heat flux published by researchers, the predictions that were obtained were acceptable. The main cause of the deviations of the predicted heat fluxes from the measured values was localised variations in combustion as a result of the positions of the fuel spray plumes relative to the measurement point. It was also concluded that combustion affected the gas flow processes with particular reference to squish as the initial high rise in pressure at the start of combustion which tended to occur shortly before TDC created a substantial pressure differential between the piston bowl and the gas zone sandwiched between the piston crown and the cylinder head. The reverse squish was therefore amplified considerably. The present gas flow model did not include any terms that responded directly to this phenomenon as the cylinder pressure was assumed to be uniform throughout the cylinder. In further research with this model it is recommended that additional terms be introduced into the momentum flux equations to account for the effects of injection and combustion.

Acknowledgements

The author acknowledges the funding of the project by the National Engergy Counsil of South Africa and the provision of assistance by BP (SA) and ADE (Pty) Ltd. The author expresses his appreciation to Dr C E Goering, University of Illinois, USA and Prof P Meiring, University of Natal for their encouragement and helpful discussions.

References

1. Lilly L. C. B., 1984. Diesel engine reference book. Publ. Butterworths, London, England.

2. Goering, C. E., 1986. Engine and tractor power. PWS Publishers, Boston, Massachusetts, USA.

3. Morel, T., Wahiduzzaman, S., Tree, D. R. and DeWitt, D. P., 1987. Effect of speed, load and location on heat transfer in a diesel engine – measurements and predictions. SAE paper 870154.

4. Borman, G. and Nishiwaki, K., 1987. Internal-combustion engine heat transfer. Prog. Energy Combust. Sci., 13; 1-46.

5. Callahan, T. J., Yost, D. M. and Ryan, T. W., 1985. Acquisition and interpretation of diesel engine heat release data. SAE paper 852068.

6. Hansen, A. C., 1992. A diagnostic quasi-dimensional model of heat transfer applied to a motored compression-ignition engine. SAE Paper No. 920542.

7. Eichelberg, G., 1939. Some new investigations on old combustion engine problems. Engineering, 148:463-464, 547-560.

8. Annand, W. J. D., 1963. Heat transfer in the cylinders of reciprocating internal combustion engines. Proc. IMechE, 177: 973-996.

9. Woschni, G., 1967. A universally applicable equation for the instantaneous heat transfer coefficient in the internal combustion engine. SAE paper 670931.

10. Morel, T. and Keribar, R., 1985. A model for predicting spatially and time resolved convective heat transfer in bowl-in-piston combustion chambers. Trans. SAE paper 850204, 94: 2.77-2.93.

11. Szekely, G. A. and Alkidas, A. C., 1986. A two-stage heat release model for diesel engines. SAE paper 861272.

12. Borgnakke, C., Davis, G. C. and Tabaczynski, R. J., 1981. Predictions of in-cylinder swirl velocity and turbulence intensity for an open chamber cup in piston engine. Trans. SAE paper 010224, 90: 964-978.

13. Murakami, A., Arai, M. and Hiroyasu, H., 1988. Swirl measurements and modelling in direct injection diesel engines. SAE paper 880385.

14. Faletti, J. J., Sorenson, S. C. and Goering, C. E., 1982. Energy release rates from hybrid fuels. ASAE paper 82-1548.

15. Taylor, A. B., 1987. Combustion quality of selected compression-ignition fuels. Unpubl. M Sc.Eng thesis, Dept. of Agric. Eng., Univ. Natal, Pietermaritzburg, RSA.

16. Hansen, A. C., 1991a. Modelling gas flow in a direct injection diesel engine: I – squish and swirl. R & D Journal 7(2), 16-24.

17. Hansen, A. C., 1991b. Modelling gas flow in a direct injection diesel engine: II – turbulence. R & D Journal 7(2), 25-31.

18. Kunitomo, T., Matsuoka, K. and Oguri, T., 1975. Prediction of radiative heat flux in a diesel engine. SAE paper 750786.

19. Kamel, M. and Watson, N., 1979. Heat transfer in the indirect injection diesel engine. SAE paper 790826.

20. Chang, S. L. and Rhee, K. T., 1983. Computation of radiation heat transfer in diesel combustion. SAE paper 831332.

21. Abu-Romia, M. M. and Tien, C. L., 1967. Appropriate mean absorption coefficients for infrared radiation of gases. Trans. ASME, J. Heat Transfer, 89:321-327.

22. Morel, T., and Keribar R., 1986. Heat radiation in DI diesel engines. SAE paper 860445.

23. Taylor, A. B., Hansen A. C., Lyne, P. W. L. and Meiring, P., 1989. Engine stress from combustion of alternative fuels in compression-ignition engines. Final Report prepared for National Energy Council, Pretoria, RSA.

24. Hansen, A. C., Taylor, A. B., Lyne, P. W. L. and Meiring, P., 1989. Alternative fuels combustion and performance monitor for C-I engines. Final Report prepared for National Energy Counil by Dept. of Agri. Eng., Univ. Natal, Pietermaritzburg, RSA.

25. Annand, W. J. D. and Ma, T. H., 1970. Instantaneous heat transfer rates to the cylinder head surface of a small compression-ignition engine. Proc. I. Mech. E., 185:976-987.

26. Dent, J. C. and Sulaiman, S. J., 1977. Convective and radiative heat transfer in a high swirl direct injection diesel engine. SAE paper 770407.

27. Van Gerpen, J. H., Huang, C. and Borman, G. L., 1985. The effect of swirl and injection parameters on diesel combustion and heat transfer. SAE paper 850265.